GEOPHYSICS, VOL. 68, NO. 1 (JANUARY-FEBRUARY 2003); P. 108–117, 11 FIGS., 1 TABLE.
10.1190/1.1543198

Velocity-permeability relations within hydraulic units

Manika Prasad*

ABSTRACT

Relationships between seismic velocity and permeability have been difficult to establish. I show that by grouping and sorting rocks into hydraulic units, we can establish relationships between velocity and permeability. The hydraulic units are calculated from measured porosity and permeability values. Correlation between velocity and permeability is significant within each hydraulic unit (the correlation coefficient, R^2, lies in the range 0.65–0.87). This correlation is an extension of the match between porosity and permeability within a hydraulic unit. I show how the compaction and cementation history of a sediment can have effects on its physical properties such as porosity and permeability and on its seismic properties. The measured velocity data are further approximated with the Biot model. The velocity-permeability relation and modeling results are demonstrated for a large data set of laboratory measurements. The good match between calculated and measured data demonstrates that this relation can be used to predict permeability from velocity in well logs by zoning the data from training wells into hydraulic units. One possible application is shown where, by using site-specific data, the velocity-permeability relation is vastly improved with a correlation coefficient R^2 of 0.9.

INTRODUCTION

Knowledge about porosity and permeability is essential to evaluate fluid content, fluid flow, and recovery rates in a formation. Information about subsurface formations is generally gathered at three different scales, which vary in resolution, spatial coverage, and number of parameters measured. There is a need to scale up or down to increase reliability of prediction. For example, seismic mapping yields information about subsurface structures and seismic velocities in the formation. It has least resolution (several meters) but maximum coverage (tens of kilometers). This is by far the largest data set available to us, where compressional wave velocity (V_p) is the main measured property. Well logging yields, among other things, information on subsurface formation velocity and porosity. It has medium resolution (several centimeters) and coverage (several meters). The number of measured properties is increased to include, for example, porosity, shale volume, and electrical resistivity, in addition to V_p. In few cases, nuclear magnetic resonance logs and Stoneley wave analyses are used to yield permeability values. Laboratory measurements on cores yield, for example, velocity, porosity, and permeability at discrete depths in the formation. These investigations deliver maximum resolution (millimeter-micrometer) but minimum coverage (centimeters). A large number of properties can be measured, for example, V_p, shear wave velocity (V_s), P- and S-wave attenuation (Q_p^{-1} and Q_s^{-1}), porosity, permeability, density, mineralogy, and microstructure.

Thus, velocity and porosity are well studied; however, information about permeability, particularly in-situ permeability, is sparse. In absence of measured values of permeability and porosity, proxies are used to infer these parameters from indirect measurements. Attempts to predict permeability from porosity have not been very successful. Similarly, although empirical relations exist for velocity-porosity transforms (for example, Raymer et al., 1980; Nur et al., 1995), establishing a relation between permeability and velocity has met with very little success. It has been shown theoretically that both porosity and permeability control wave propagation in porous rocks (for example, Biot, 1956a, b). Practical application of these theories is precluded by a lack of "correct" choice of the required pore space parameters. A complete description of the pore space parameters will help us to characterize reservoir formations and to understand and model wave propagation mechanisms in porous media. Such a relation will also increase reliability of permeability predictions from velocity.

Presented at the 69th Annual International Meeting, Society of Exploration Geophysicists. Published on Geophysics Online July 30, 2002. Manuscript received by the Editor July 25, 2000; revised manuscript received July 19, 2002.
*Stanford University, SRB Project, Geophysics Department, 397 Panama Mall, Stanford, California 94305-2215. E-mail: manika.prasad@stanford.edu.

Since both velocity and permeability are governed by volumetric *and* geometric considerations, whereas porosity is only a volumetric description, a common link between the three will require some description and quantification of pore space geometry. Amaefule et al. (1993) have shown that a relationship between permeability and porosity exists once the data are separated in hydraulic units. Since velocity depends on pore space volume as well as geometry, I examine the nature of a relation between permeability and velocity. Such a relation is invaluable as a prediction tool. For example, using laboratory data as training data, hydraulic units can be identified in the area of interest. Within these hydraulic units, permeability can be predicted using porosity and velocity from the sonic logs and seismic data. In this paper, I extend the relation between porosity and permeability to the seismic properties of velocity and quality factor using laboratory data. I further show a theoretical basis for this empirical relation between seismic properties, permeability, and porosity.

METHODOLOGY

Many attempts have been made in the past to predict permeability from porosity. Lack of correlation between predicted and measured permeability underscores the difficulties involved in such predictions. The uncertainty is because porosity, by definition, is a volumetric parameter; it is the ratio of pore volume to bulk volume. Permeability, on the other hand, is a measure of the flow properties of a fluid through the pores, which depends not only on the volumetric proportion of the pore space, but also on its geometric distribution and connectivity. Thus, a porosity-permeability relation will be a function of the pore geometry. Various researchers have attempted to model pores with geometrical shapes. The most commonly used porosity-permeability relation is the Kozeny-Carman relation derived for parallel capillary tubes:

$$k = \frac{1}{2\tau^2 S_{Vgr}^2}\frac{\phi^3}{(1-\phi)^2}, \tag{1}$$

where k = permeability (in μm^2), ϕ = fractional porosity, τ = tortuosity, and S_{Vgr} = specific surface area per unit grain volume (Kozeny, 1927; Carman, 1937). In equation (1), the factor 2 accounts for the assumption that the pores are cylindrical with circular cross-sections. Some authors (for example, Paterson, 1983; Walsh and Brace, 1984; Amaefule et al., 1993) generalized this equation to include different pore shapes (F_s). In the notation of Amaefule et al. (1993),

$$k = \frac{1}{F_s\tau^2 S_{Vgr}^2}\frac{\phi^3}{(1-\phi)^2}. \tag{2}$$

Equations (1) and (2) are only partially successful in predicting permeability from porosity. Most pores are not circular cylinders and so equation (1) has limited applicability. Information on τ, S_{Vgr}, and F_s is not readily available and so equation (2) is difficult to apply. Amaefule et al. (1993) have shown that after some rearrangement, equation (2) can be simplified to

$$\log \mathrm{RQI} = \log \mathrm{FZI} + \log \varepsilon, \tag{3}$$

where ε is the void ratio, the ratio of pore volume to solid volume, defined as

$$\varepsilon = \frac{\phi}{(1-\phi)}, \tag{4}$$

RQI is the reservoir quality index. With permeability expressed in mD, it is defined as

$$\mathrm{RQI} = 0.0314\sqrt{\frac{k}{\phi}}. \tag{5}$$

FZI is the flow zone indicator, expressed as

$$\mathrm{FZI} = \frac{1}{\sqrt{F_s}\tau S_{Vgr}}. \tag{6}$$

In equation (3), the parameters which define pore space (F_s, τ, and S_{Vgr}) are grouped together as FZI. Clearly, FZI can be calculated from a set of measured laboratory data on porosity and permeability:

$$\mathrm{FZI} = \frac{0.0314}{\varepsilon}\sqrt{\frac{k}{\phi}}. \tag{7}$$

This term can be understood as the relation between the volume of void space (ε) and its geometric distribution (RQI). Rocks with FZI values within a narrow range belong to one hydraulic unit; that is, they have similar flow properties. Amaefule et al. (1993) used this relation to show that samples with similar FZI values plot together on a semilog plot of porosity versus permeability and that the porosity-permeability relation can be defined uniquely in each hydraulic unit. They also show how permeability variations in a reservoir can be understood by binning its cored data in hydraulic units that have similar FZI values calculated using equation (7).

In this paper, I first test this concept of grouping porosity and permeability data according to their FZI units. I then show that this relation can be extended to seismic parameters to create a strong correlation between velocity and permeability. Finally, the FZI units are used in theoretical analysis to model velocity and quality factor.

Porosity analyses

The laboratory data used for this study were compiled by Prasad (1998; 1999) and are given in Appendix A. The data were chosen such that they included velocity and attenuation measurements at similar pressures along with porosity and permeability values.

Figure 1 shows a plot of the porosity-permeability variations in this data set. No apparent relation is observed in Figure 1a. In Figure 1b, the data are color coded according to FZI units calculated from equation (7). The different colors denote FZI intervals as shown by the legend. Separation in hydraulic units (intervals with same FZI values) can be made according to the main FZI intervals present in the data. The solid lines in Figure 1b were calculated from Equation (7) using FZI values marked on the lines. Note that in Figure 1b, lines of constant FZI plot close together at low porosity and are widely separated at higher porosities. Porosity and permeability correlate very well within an FZI interval. At the same porosity, samples with higher FZI have higher permeability. Thus, the FZI values can be understood to denote connectivity; given the same

volumetric amount of pore space, a higher connectivity would produce a larger permeability along with higher FZI.

Velocity analyses

Prasad (1998) has shown that the velocity-porosity relation (Figure 2, open symbols) can be improved by using the modified porosity concept of Galmudi et al. (1999) (Figure 2, closed symbols). Modified porosity takes into account that, in clay-rich rocks, the measured porosity is lower than the total porosity, because the unconnected pore space within clay minerals is underestimated. Galmudi et al. (1999) suggest that the clay porosity (porosity of clay, 0.6, factorized by the clay content) should be added to the measured rock porosity. In Figure 2, the measured porosity data are plotted with open symbols, closed symbols mark modified porosity, modified by assuming a clay porosity of 60% as suggested by Galmudi et al. (1999). Although the scatter in the velocity-modified porosity relation is reduced, it is still significant. Note that the scatter will not decrease by changing the clay porosity. This scatter is due to the geometric distribution of the mineral grains and the pore space. Also plotted in Figure 2 are the upper and lower Hashin-Shtrikman (1963) bounds on velocity in a binary quartz-water system. These bounds describe velocity variations between two endpoints, one at zero porosity, where the velocity is that of quartz, and the other at 100% porosity, where rock velocity is that of water. The lower bound describes the softest arrangement with the water being load-bearing, and the upper bound describes the stiffest arrangement with the quartz being load-bearing. The actual arrangement of the two components can lie between these two extremes. In Figure 2, the remaining scatter in the velocity-porosity relation after accounting for porosity in the clay minerals is mainly due to the geometric distribution of the grains and pore space.

We now consider the velocity-permeability relation (Figure 3). This figure mimics the porosity-permeability plot in Figure 1. No apparent relation between permeability and velocity is observed in the raw data (Figure 3a). Figure 3b, with colorcoding as in Figure 1b, shows a clear relation between velocity and permeability within narrow confines of FZI units. Separation in different hydraulic units can be made by statistical analyses of the data. The lines in Figure 3b are regression fits between velocity and permeability within a hydraulic unit. Coefficient of determination (R^2) for all lines lies between 0.65 and 0.87. Certainly, narrower intervals could be defined for a larger data set that would improve the correlation. The correlation can also be improved by taking additional constraints, such as lithology, facies, etc.

Attenuation analyses

An important rock property that influences wave propagation is the attenuation of seismic energy. It is a measure of the loss of energy per cycle to peak strain energy stored in the sample. Although attenuation is strongly influenced by pore geometry, a correlation between attenuation and porosity (Figure 4) and between attenuation and permeability (Figure 5) is not as obvious as that for velocity. In Figure 4, although attenuation increases with increasing porosity, the large scatter is not reduced, even after accounting for the additional clay porosity.

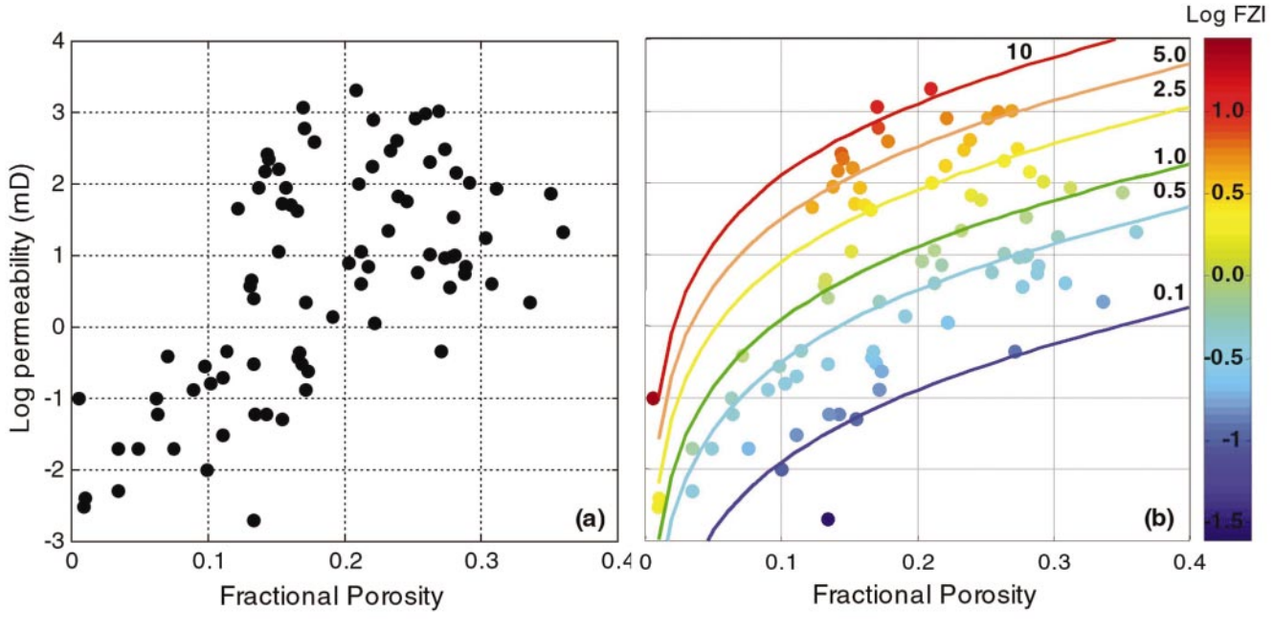

FIG. 1. Porosity-permeability relation without color codes (a) and with FZI intervals marked by different colors (b). The legend on the right gives the binning criteria for the hydraulic intervals. The raw data in (a) do not show any apparent relation. In (b), on the other hand, clear relations can be observed between porosity and permeability within narrow FZI intervals. The solid lines mark permeability calculated from equation (7) using FZI values as marked. Note that the color FZI code is in log scale: log 10 = 1, log 5 = 0.699, log 2.5 = 0.398, log 1 = 0, log 0.5 = −0.301, log 0.1 = −1.0.

A relationship between attenuation and permeability is not readily apparent in Figure 5. Although there is some separation of the data according to the hydraulic units, a clear relation cannot be established. An explanation for this behavior is found by comparing the measured data with modeling results from the Biot theory, as discussed later.

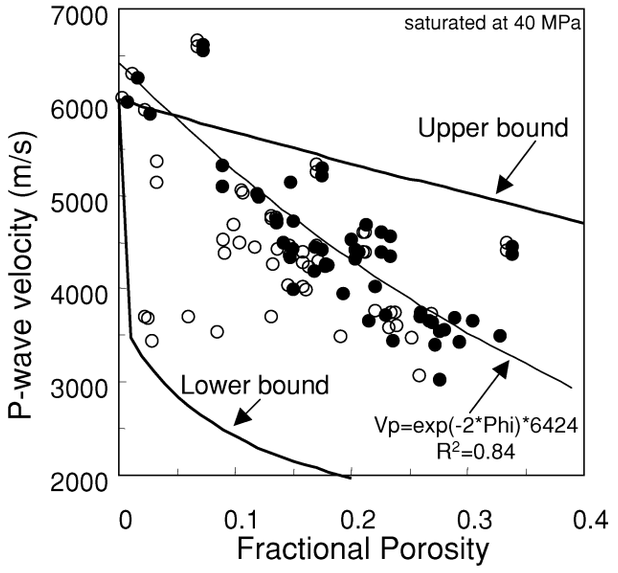

FIG. 2. Velocity-porosity relation. Open symbols denote measured porosity, solid symbols represent porosity modified by accounting for the inaccessible clay porosity. The gray solid line is an exponential fit through the solid symbols. The solid black lines are the Hashin-Shtrikman upper and lower bounds calculated for a quartz-water system. Note that some points lie above the upper bound, because they are either pure carbonates or they contain significant amounts of calcite and/or dolomite.

DISCUSSION

To understand the good correlation between velocity and permeability as observed in Figure 3b, we first examine the FZI unit. By definition, it is a product of pore parameters [shape factor (F_s), tortuosity (τ), and specific surface area to grain volume ratio (S_{vgr})] and describes connectivity between pores (larger FZI implies higher connectivity). In simple terms, it can be understood to describe the initial lithology of a sediment and its compaction and lithification history. In an ideal compaction environment, without sediment influx and cementation effects, porosity reduction is only due to overburden or pressure increase. Porosity-permeability relations follow unambiguous trends governed by initial lithological configurations (for example, grain shape, sorting, clay content). Without external influences, this relation is unique during the compaction history of the sediment. Addition of clay, diagenetic alteration and leaching out of constituent minerals, and cementation of grains, for example, will lead to deviations from this norm. Such deviations will affect both porosity and permeability. Early cementation will keep porosity and permeability at higher than normal values. Pore connectivity and FZI values will be high in such samples. On the other hand, clays deposited in pore spaces will reduce porosity and permeability. Pore connectivity and FZI values will be low in such samples.

Figure 6 shows an example of the evolution of marine clay-rich sediments from deposition to burial and lithification.

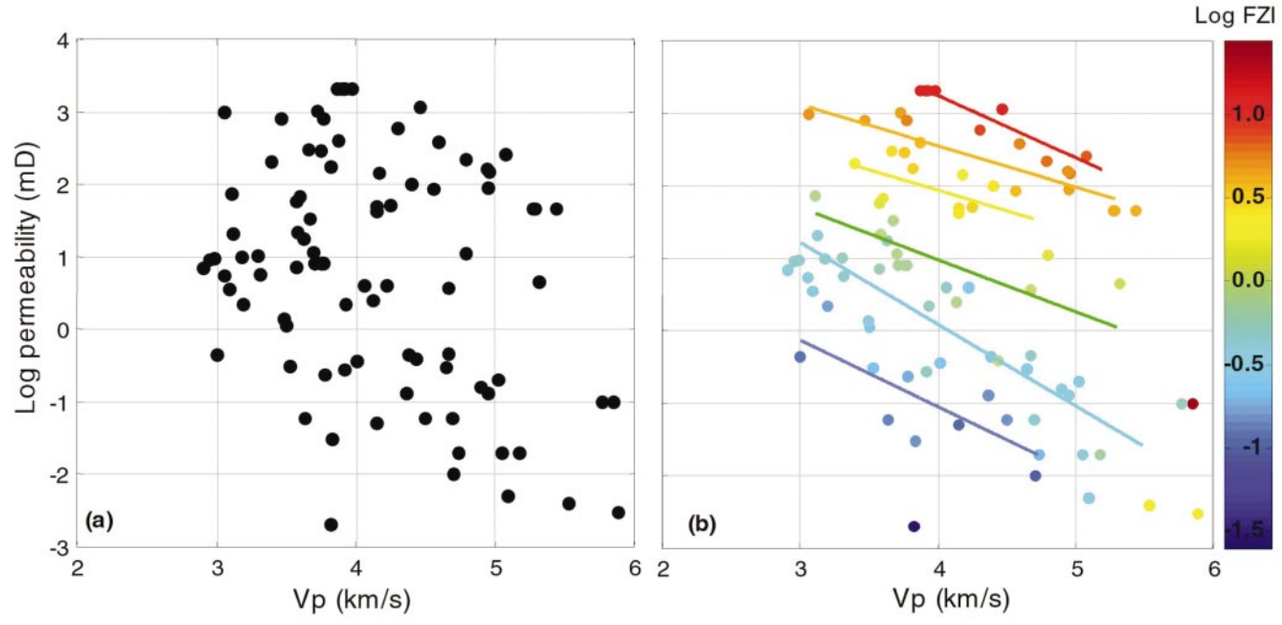

FIG. 3. Velocity-permeability relation without color codes (a) and with FZI intervals marked by different colors (b). Color codes are same as in Figure 1b. There is a clear relation between velocity and permeability. Solid lines are best fits through all data within each hydraulic unit and have a goodness of fit (R^2) greater than 0.65.

As the sediment is depositedand undergoes compaction, it will move along a normal compaction trend. Without external influences, the porosity reduction (along curve A–B) will be determined only by compaction and volume reduction due to expulsion of water/air from the pores. In Figure 6, line A–B is an empirical fit to the data. The normal compaction curve (A–B in Figure 6) is constructed from log data for marine silty clay sediments from ODP Leg 161, Site 977 (Shipboard Scientific Party, 1996). Similar compaction curves can be constructed for various sedimentary environments. Within a specific environment, pore space evolution will be more or less similar and the sediments will have the same FZI values. Now, if at a given time (= depth) during its history, the sediment experiences cementation, then the porosity trend will deviate from the normal compaction curve. In Figure 6, point D marks the onset of cementation. At this point, the porosity is "locked-in." The sediment develops a frame that resists compaction. Porosity reduction will be slower and will move along the hypothetical line D–D′. Similarly, an influx of pore-filling materials in the sediment column will reduce porosity below the normal compaction curve, shown by the hypothetical line C–C′. For both scenarios C–C′ and D–D′, the pore space parameters, or FZI units, will differ from those along the line A–B.

An analogous evolution curve for velocity with depth is shown in Figure 7. Velocity increase with depth progresses along line A–B. Regression curves for velocity logs from the same site as in Figure 6 were used to construct this velocity curve. At the onset of cementation, shown schematically at point D, there is a jump in velocity due to the change in

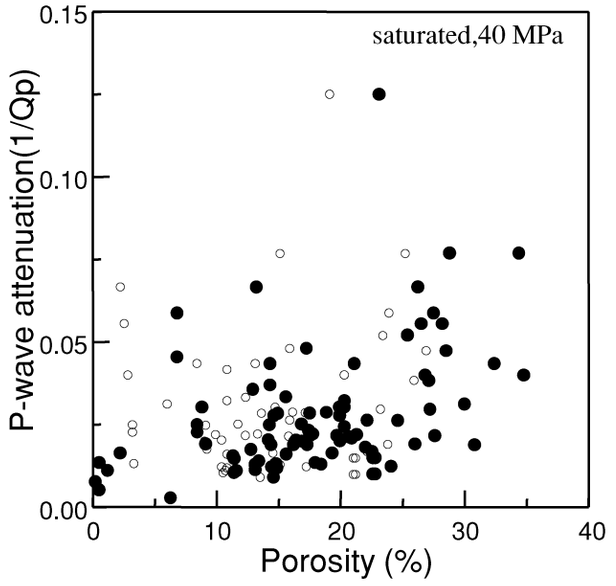

FIG. 4. Attenuation as a function of porosity. Open symbols represent measured porosity, and solid symbols represent porosity modified by accounting for the inaccessible clay porosity. There is large scatter in the data, but low porosity samples appear to have lower attenuation.

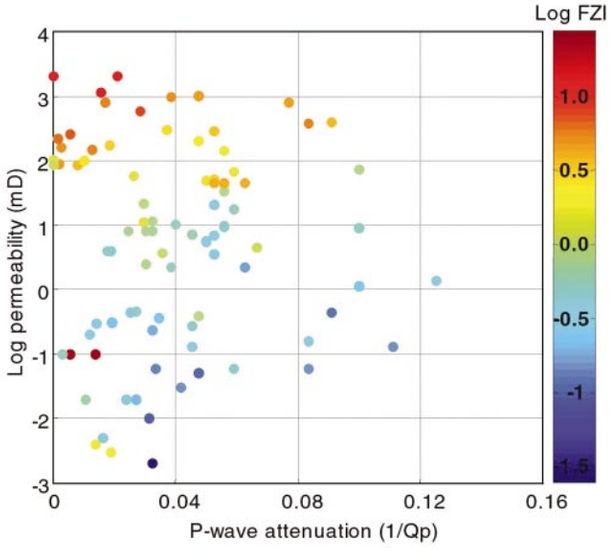

FIG. 5. Attenuation-permeability relation. Color codes are same as in Figure 1b. Numbers marks FZI intervals. A clear relation between attenuation ($1/Q_p$) and permeability is not apparent.

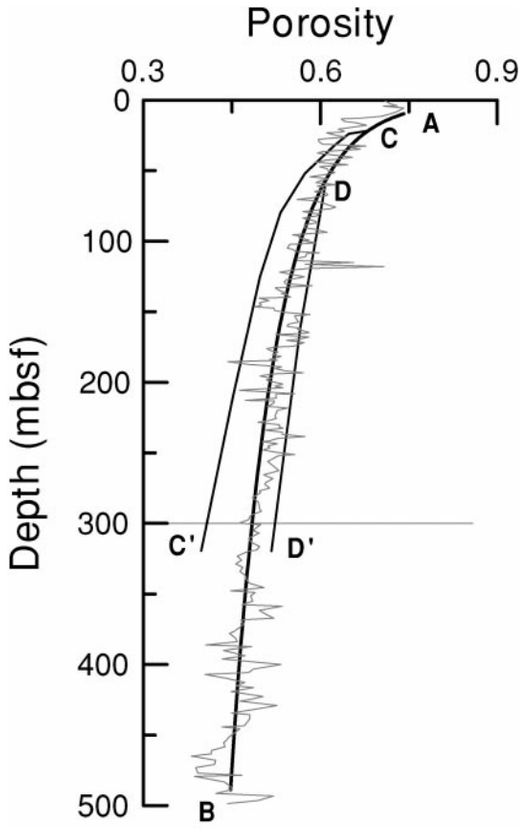

FIG. 6. Porosity change with depth (A–B). The smoothed data are taken from logging results of Site 977, ODP Leg 161 (Shipboard Scientific Party, 1996). Line C–C′ shows hypothetical porosity-depth relation after influx of pore filling materials at point C, and line D–D′ shows hypothetical porosity changes with depth after initial cementation has locked-in porosity at point D.

compressibility. Now the velocity-depth curve moves along D–D′. Similarly, if there is an influx of pore-filling materials, the velocity in the sediment will move along curve C–C′. The pore-space configuration and, with it, the porosity-permeability and the velocity-permeability relations along the different compaction-cementation histories (A–B, A–C–C′, and A–D–D′) will be unique. They can be grouped together by the FZI units that account for pore space configurations. These cementation and pore-filling variations in velocity and porosity have been observed, for example, in a silty environment (Prasad and Dvorkin, 2001) and in a carbonate deposition basin (Urmos et al., 1993).

Permeability estimates made with equation (7) with porosity values from Figure 6 and hypothetical FZI values are shown in Figure 8. The dark and light gray curves in Figure 8 are calculated from log porosity and FZI values of 0.1 (light gray) and 0.25 (dark gray) to show their effect on permeability. For example, the cementation event will have a high FZI value, whereas a pore-filling event will lead to a reduction in FZI values. As in the previous Figures 6 and 7, the normal compaction curve is marked by A–B. Early cementation event and subsequent compaction is traced by D–D′, whereas C–C′ traces a pore-filling event.

Theoretical considerations

I used the Biot theory (Biot, 1956a, b; Stoll, 1980) to model velocity and attenuation for data from Prasad (1998) and for a hypothetical material consisting of quartz particles. Biot's model describes wave propagation in a two-phase system: a porous elastic frame and a viscous, incompressible pore fluid. The losses are due to relative motion between the frame and the pore fluid. Thus, velocity and attenuation are functions of the frame properties, the solid and the pore fluid moduli, and of pore space parameters such as porosity, permeability, pore size, structure constant, and mass-coupling effects. These pore space parameters (for example, structure constant and mass coupling between grains and pore fluid) are difficult to measure. Various studies have attempted to isolate the effect of each of these parameters by keeping all others constant (e.g., Hovem and Ingram, 1979; Dunlop, 1988). The applicability of such an approach is limited because of strong interrelations between the various pore space parameters. I used FZI units to describe pore space parameters.

The calculations presented here were made for quartz mineralogy. The frame modulus was estimated from mineral modulus of quartz and by assuming critical porosity = 36% (Nur et al., 1995). Permeability was calculated from equation (7) for FZI

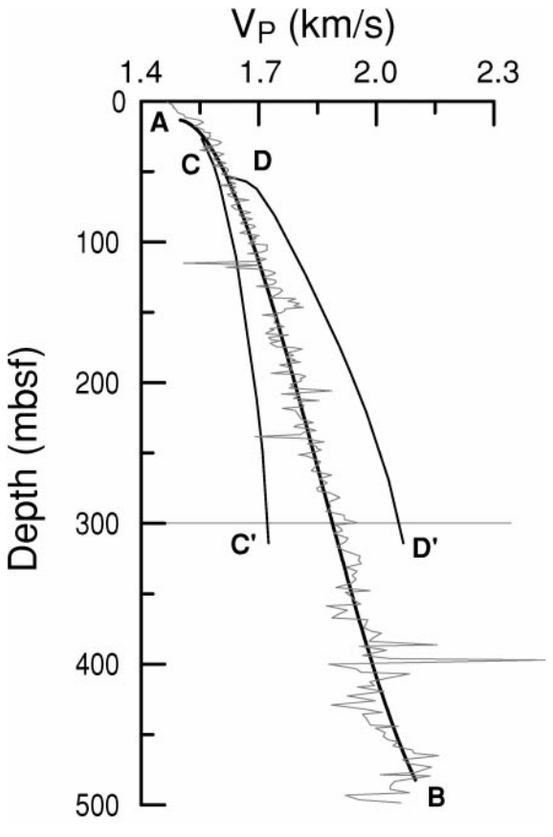

FIG. 7. Velocity change with depth (A–B). The smoothed data are taken from logging results of Site 977, ODP Leg 161 (Shipboard Scientific Party, 1996). Line C–C′ shows hypothetical velocity-depth relation after influx of pore-filling materials at point C and line D–D′ marks hypothetical velocity changes with depth at the onset of initial cementation (point D).

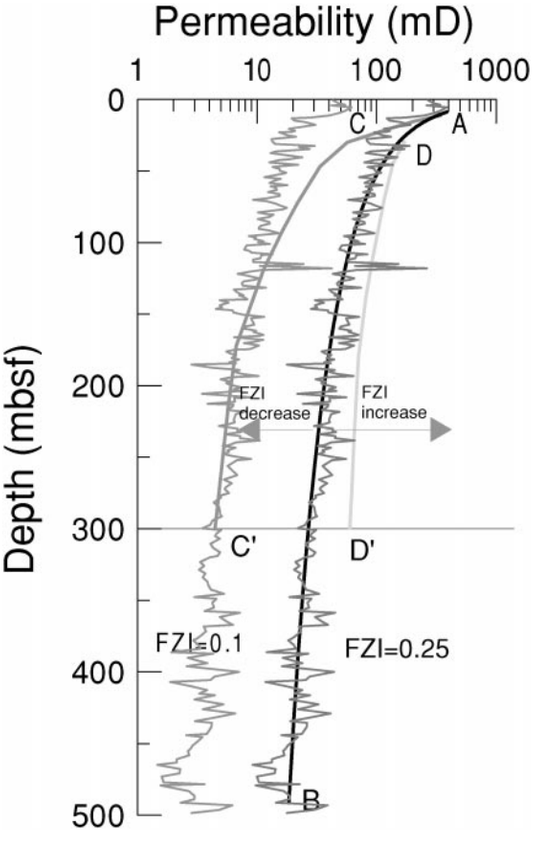

FIG. 8. Permeability change with depth (A–B) calculated from log porosity using an FZI value of 0.25. C–C′ shows hypothetical permeability-depth relation after influx of pore-filling materials at point C where FZI is decreased to 0.1. Line D–D′ marks a hypothetical permeability change with depth at the onset of initial cementation at point D.

values of 0.1, 0.25, 0.75, and 2.5 and porosity values varying between 5% and 35%. The pore-filling medium was assumed to be water. Input parameters for the model are given in Table 1.

The velocity and attenuation variations with permeability are shown in Figures 9 and 10, respectively. The color codes in both figures are same as in Figure 1. There is good agreement between the calculated velocity (solid lines) and the data from Figure 3 (symbols). Within each hydraulic unit, the model predicts velocity variations with permeability fairly well. Although the theoretical attenuation predictions do not appear very successful, they reveal important insights. As noted by Winkler (1985) and Prasad and Meissner (1992), the Biot model predicts attenuation values that are much lower than measured values, mainly because additional loss mechanisms such as frame and squirt-flow attenuations are also active. The model predicts higher losses for larger FZI values. In the model, for each FZI value, there is a peak in attenuation at a certain permeability value. With decreasing FZI value, the attenuation peak decreases and moves towards lower permeability values. Thus with all other parameters kept constant, position and magnitude of this peak is governed by the pore space parameters, represented by FZI values. This is understandable, since the Biot loss mechanism is due to relative flow between solid grains and pore fluid. Having additional permeability and attenuation data available should allow us to better define the nature of the relation between them. Specifically, by measuring samples with same FZI but controlled permeability (for example, in pressure dependent velocity, attenuation, and permeability measurements), we should be able to track such changes. Furthermore, combining Biot losses with frame and squirt-flow loss mechanisms will allow us to make realistic estimates of attenuation in rocks.

Table 1. Biot equations for longitudinal waves as functions of strain of the frame (e) and displacement of the fluid relative to the frame (ξ), and list of input parameters used in these equations.

Biot equations for longitudinal waves

$$\Delta^2(He - C\xi) = \partial^2/\partial t^2(\rho_e e - \rho_f \xi)$$
$$\Delta^2(Ce - M\xi) = (\rho_f e - m\xi) - \eta F(\kappa)/k\,\partial\xi/\partial t$$

H, C, M are elastic moduli, defined by Stoll (1980) as

$$H = \frac{(K_S - K_{dry})^2}{D - K_{dry}} + K_{dry} + \frac{4}{3}\mu, \quad C = \frac{K_S(K_S - K_{dry})}{D - K_{dry}},$$

and $$M = \frac{K_S^2}{D - K_{dry}}, \text{ where } D = K_S\left(1 + \phi\frac{K_S}{K_f} - \phi\right)$$

Parameter	Description	Value or equation used
ϕ	Fractional porosity	Between 0.1 and 0.35
ϕ_c	Critical porosity	0.36 (Nur et al., 1995)
ρ_e	Bulk density	$(1\text{-}\phi)\rho_s + \phi\rho_f$
ρ_f	Fluid density	1.0 g/cm^3
ρ_s	Mineral density	2.65 g/cm^3
ρ_{dry}	Dry frame density	$(1\text{-}\phi)\rho_s$
K_s	Mineral bulk modulus	37 MPa
μ_s	Mineral shear modulus	44 MPa
K_f	Fluid bulk modulus	2.22 MPa
η	Fluid viscosity	0.2 cp
f	Frequency	10 Hz, 1 kHz, 1 MHz
ω	Circular frequency	$= 2\pi f$
K_{dry}	Frame bulk modulus	$K_{dry} = K_s(1\text{-}\phi/\phi_c)$ (Nur et al., 1995)
μ_{dry}	Frame shear modulus	$\mu_{dry} = \mu_s(1\text{-}\phi/\phi_c)$ (Nur et al., 1995)
FZI	Flow zone indicator	Between 0.1 and 2.5
k	Permeability (mD)	Calculated with equation (7)
a	Pore size	$a = 1.8081 \times k^{0.3932}$
m	Mass coupling factor	$m = c\rho_f/\phi$
c	Shape factor	$c = 1/\text{FZI}$
$F(\kappa)$	High-frequency correction factor	
κ		a sqrt $(\omega\rho_f/\eta)$

APPLICATIONS

In Figure 11, I show the velocity-permeability trend from Figure 3 again, but with more data values added to the plot. These data are taken from laboratory measurements of core samples from three different wells. Although the data are from very different environments, the velocity-permeability variation is governed by same pore space geometry. From Figure 11, we can derive the following information:

1) All data fall within narrow confines of predefined hydraulic units.
2) The V_p-permeability relation can be improved for each specific site. This is mainly achieved by narrowing down the hydraulic unit boundaries. An exponential fit through a subset of the data around FZI = 1.0 had a correlation coefficient (R^2) = 0.92.
3) Such data can be used to establish flow properties within a reservoir. Then, using the velocity-permeability relation

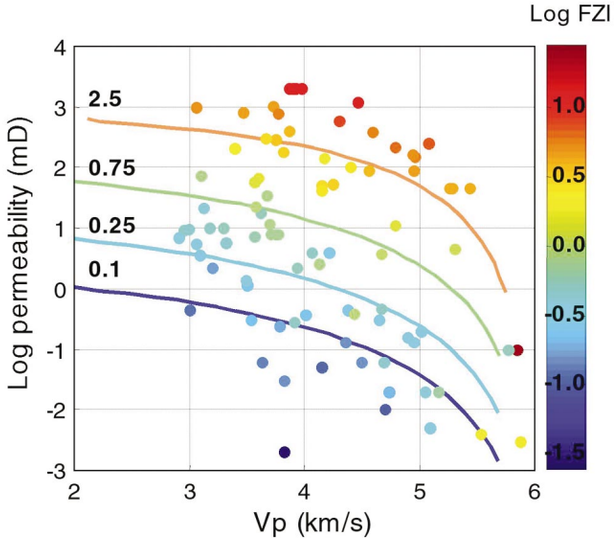

FIG. 9. Velocity-permeability relation. Color codes are same as in Figure 1b. Symbols represent measured data, solid lines mark values calculated by the Biot model. The calculations were made for FZI values of 2.5, 0.75, 0.25, and 0.1 (corresponding to log FZI of 0.398, −0.125, −0.602, −1.0). There is a remarkable agreement between measured and predicted values.

(such as the one established in Figure 11), we can predict and control changes either spatially (in the case of a new field) or temporally (in a producing field).

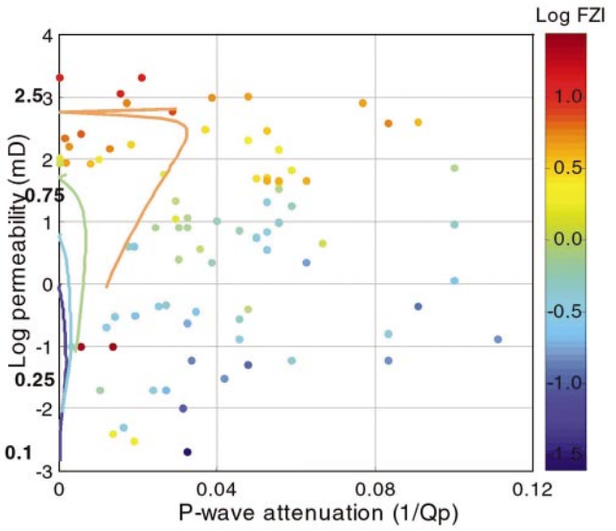

FIG. 10. Attenuation-permeability relation. Color codes are same as in Figure 1b. Symbols represent measured data, solid lines mark values calculated by the Biot model. The different lines represent calculations for FZI values as marked by numbers on the lines. The calculations were made for FZI values of 2.5, 0.75, 0.25, and 0.1 (corresponding to log FZI of 0.398, −0.125, −0.602, −1.0). Although, the model predictions lie within measured range for FZI = 2.5 (blue line), they are much lower for the lower FZI values.

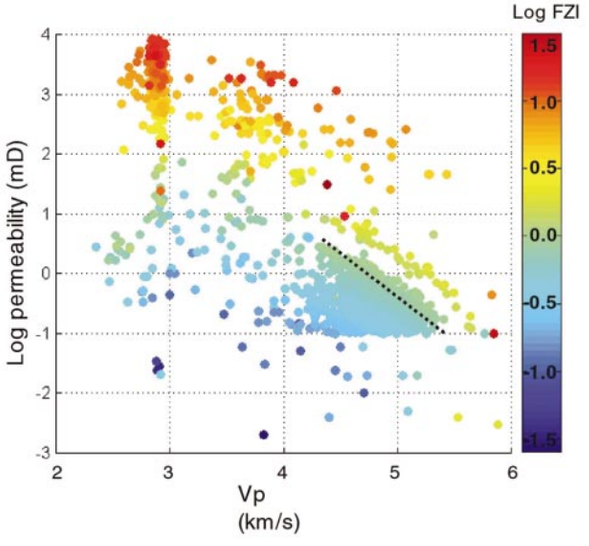

FIG. 11. Velocity-permeability relation for additional data sets from different environments. Color codes are same as in Figure 1b. The new data are from a tight sand reservoir, marine reservoir sand, and from a data collection of reservoir type sandstones. The black line marks an exponential fit through a subset of the data around FZI = 1.0 with log permeability (mD) = $-0.002999 \times V_p$ (m/s) + 15.55; $R^2 = 0.92$.

CONCLUSIONS

Using a collection of velocity, porosity, and permeability data from various sources, I have shown that, by grouping the data in different hydraulic units based on pore space properties, a positive correlation between velocity and permeability can be established. The pore space parameters, grouped together as FZI values, are calculated from measured values of porosity and permeability. By using FZI values for pore space properties, velocity modeled with the Biot theory agrees well with measured data and attenuation is underpredicted. I further show how, by defining hydraulic units for a specific site, flow properties can be controlled and predicted.

ACKNOWLEDGMENTS

I thank Mario Gutierez, Emma Rasolovoahangy, Gary Mavko, Amos Nur, and the reviewers for their suggestions and discussions, and Jack Dvorkin for the core data from wells. This work was performed under the auspices of National Science Foundation (Grant No. EAR 0074330) and Department of Energy (Award No. DE-FC26-01BC15354). However, any opinions, findings, conclusions, or recommendations expressed herein are those of the author and do not necessarily reflect the views of the DOE and or the NSF.

REFERENCES

Amaefule, J. O., Altunbay, M., Tiab, D., Kersey, D. G., and Keelan, D. K., 1993, Enhanced reservoir description: Using core and log data to identify hydraulic (flow) units and predict permeability in uncored intervals/wells: SPE Paper 26436, 1–16.

Assefa, S., and Sothcott, J., 1997, Acoustic and petrophysical properties of seafloor bedrocks: SPE Formation Evaluation, **12**, no. 3, 157–163.

Biot, M. A., 1956a, Theory of propagation of elastic waves in fluid saturated porous solids. I: Low frequency range: J. Acous. Soc. Amr., **28**, 168–178.

———1956b, Theory of propagation of elastic waves in fluid saturated porous solids. II: High frequency range: J. Acous. Soc. Am., **28**, 179–191.

Carman, P. C., 1937, Fluid flow through granular beds: Trans. AIChE, **15**, 150–166.

Dunlop, J., 1988, Propagation of acoustic waves in marine sediments: Exp. Geophys., **19**, 513–535.

Galmudi, D., Dvorkin, J., and Nur, A., 1999, Elastic-wave velocities in sandstones with nonload-bearing clay: Geophys. Res. Lett., **26**, 939–942.

Hashin, Z., and Shtrikman, S., 1963, A variation approach to the elastic behavior of multiphase materials: J. Mech. Phys. Solids, **11**, 127–140.

Hovem, J. M., and Ingram, G. D., 1979, Viscous attenuation of sound in saturated sand: J. Acous. Soc. Am., **66**, 1807–1812.

Klimentos, T., and McCann, C., 1990, Relationships among compressional wave attenuation, porosity, clay content, and permeability in sandstones: Geophysics, **55**, 998–1014.

Kozeny, J., 1927, Ueber Kapillare Leitung des Wassers im Boden: Sitzungsberichte der Akademie der Wissenschaften in Wien, **136**, 271–306.

Lucet, N., 1989, Vitesse et attenuation des ondes elastiques soniques et ultrasoniques dans les roches sous pression de confinement: Ph.D. diss., Institut Français du Petrole.

Nur, A., Mavko, G., Dvorkin, J., and Gal, D., 1995, Critical porosity: The key to relating physical properties to porosity in rocks: 65th Ann. Internat. Mtg., Soc. Expl. Geophys., Expanded Abstracts, 878–881.

Paterson, M. S., 1983, The equivalent channel model for permeability and resistivity in fluid-saturated rock—A reappraisal: Mechanics of Materials, **2**, 345–352.

Prasad, M., 1998, Empirical trends in velocity and quality factor properties of reservoir rocks: 68th Ann. Internat. Mtg., Soc. Expl. Geophys., Expanded Abstracts, 992–995.

——— 1999, Correlating permeability with velocity using Flow Zone Indicators: 69th Ann. Internat. Mtg., Soc. Expl. Geophys., Expanded Abstracts, 184–187.

Prasad, M., and Dvorkin, J., 2001, Velocity-porosity transforms in marine sediments: Petrophysics, **42**, 42–47.
Prasad, M., and Manghnani, M. H., 1997, Effects of pore and differential pressures on compressional wave velocity and quality factor on Berea and Michigan sandstones: Geophysics, **62**, 1163–1176.
Prasad M., and Meissner, R., 1992, Attenuation mechanisms in sands: Laboratory versus theoretical (Biot) data: Geophysics, **57**, 710–719.
Prasad, M., Palafox, G., and Nur, A., 1999, Velocity and attenuation characteristics of Daqing sandstones: Effects of permeability on velocity and attenuation anisotropy: EOS, **80**, F963.
Raymer, D. S., Hunt, E. R., and Gardner, J. S., 1980, An improved sonic transit time-to-porosity transform: Presented at 21st Ann. Mtg., Soc. Prof. Well Log Analysts, paper P.
Shipboard Scientific Party, 1996, Site 977; *in* Comas, M. C., Zahn, R., Klaus, A., et al., Proc. Ocean Drilling Program, Init. Repts., **161**, 299–353.
Stoll, R. D., 1980, Theoretical aspects of sound transmission in sediments: J. Acous. Soc. Am., **68**, 1341–1350.
Tao, G., King, M. S., and Nabi-Bidhendi, M., 1995, Ultrasonic wave propagation in dry and brine-saturated sandstones as a function of effective stress: Laboratory measurements and modeling: Geophys. Prosp., **43**, 299–327.
Urmos, J., Wilkens, R. H., Bassinot, F., Lyle, M., Marsters, J. C., Mayer, L. A., and Mosher, D. C., 1993, Laboratory and well-log velocity and density measurements from the Ontong Java Plateau: New in-situ corrections to laboratory data for pelagic carbonates, *in* Berger, W. H., et al., Proc. Ocean Drilling Program, Scientific Results, **130**, 607–622.
Walsh, J. B., and Brace, W. F., 1984, The effect of pressure on porosity and the transport properties of rock: J. Geophys. Res., **89**, 9425–9431.
Winkler, K. W., 1985, Dispersion analysis of velocity and attenuation in Berea sandstone: J. Geophys. Res., **90**, 6793–6800.

APPENDIX A

Data used for this study were reported in Prasad (1998) and are listed in Table A-1. The source numbers in Table A-1 correspond to the following authors: 1 = Assefa and Sothcott (1997), 2 = Prasad et al. (1999), 3 = Klimentos and McCann (1990), 4 = Lucet (1989), 5 = Prasad and Manghnani (1997), 6 = Tao et al. (1995). All values in the table are given for effective pressures around 40 MPa.

Table A-1. Data used for this study.

Source number	Sample lithology	Porosity (%)	Clay (%)	*Vp* (m/s)	*Qp*	Permeability (mD)
1	dolerite	0.88	1.96	5885	53	0.003
1	gneiss	0.95	4.99	5532	74	0.004
1	gneiss	1.59	0	5931	129	0
1	sandstone	2.8	6.48	4601	18	0
1	sandstone	3.41	6.76	5171	97	0.02
1	sandstone	3.46	0	5091	62	0.005
1	sandstone	4.89	0	5048	42	0.02
1	basalt	4.99	3.17	4608	15	0
1	siltstone	5.71	6.99	4354	24	0
1	sandstone	6.36	26.2	4695	17	0.06
1	basalt	7.08	7.26	4436	21	0.39
1	sandstone	7.52	0	4735	37	0.02
1	sandstone	9.79	9.75	3917	22	0.28
1	basalt	11.08	11.4	3832	24	0.03
1	basalt	13.37	7.28	3824	31	0.002
1	sandstone	13.4	0	4126	33	2.51
1	siltstone	14.23	42	3636	30	0.06
1	siltstone	16.93	25.83	3531	52	0.31
1	sandstone	17.35	2.71	3780	31	0.24
2	sandstone	19.1	10	3488	8	1.4
2	sandstone	23.2	10	3580	34	22
2	sandstone	23.4	5	3751	19	295
2	sandstone	23.9	9	3601	17	68
2	sandstone	25.2	9	3466	13	818
2	sandstone	26.9	4	3726	21	1030
3	sandstone	2.43	0	5835	585	0
3	sandstone	2.72	0	5934	4599	0
3	sandstone	5.98	3	5225	275	0
3	sandstone	8.96	6	4947	22	0.13
3	sandstone	9.96	7	4705	32	0.01
3	sandstone	10.22	9	4895	12	0.16
3	sandstone	11.39	6	4666	37	0.46
3	sandstone	13.11	7	4666	28	3.67
3	sandstone	13.47	14	4498	12	0.06
3	sandstone	13.72	0.5	4950	613	87.65
3	sandstone	14.15	1	4960	79	150.7
3	sandstone	14.37	1	5078	185	255.9

(*Continued*)

Table A-1. (*Continued*).

Source number	Sample lithology	Porosity (%)	Clay (%)	*Vp* (m/s)	*Qp*	Permeability (mD)
3	sandstone	14.47	0.2	4788	712	220.9
3	sandstone	15.13	4	4794	34	11.06
3	sandstone	15.18	0.7	4942	394	160.4
3	sandstone	15.41	15	4246	19	52.42
3	sandstone	15.46	15	4152	21	0.05
3	sandstone	15.72	5	4564	127	87.55
3	sandstone	16.11	15	4152	20	50.51
3	sandstone	16.5	15	4149	18	41.74
3	sandstone	16.65	12	4010	29	0.37
3	sandstone	16.71	8	4381	40	0.44
3	sandstone	17.13	12	3933	26	2.21
3	sandstone	17.18	15	4362	9	0.13
3	sandstone	21.19	15	3700	31	11.42
3	sandstone	21.73	22	3572	22	7.1
3	sandstone	22.2	25	3500	10	1.13
3	sandstone	25.41	20	3314	20	5.78
3	sandstone	26.32	20	3299	25	10.27
3	sandstone	27.12	25	3000	11	0.45
3	sandstone	27.33	5	3666	27	305.8
3	sandstone	27.39	23	2952	10	9.3
3	sandstone	27.73	17	3090	19	3.5
3	sandstone	27.87	17	2990	18	9.59
3	sandstone	27.96	15	3675	18	33.67
3	sandstone	28.04	20	3181	18	10.05
3	sandstone	28.79	18	3056	20	5.47
3	sandstone	28.87	23	2909	19	7.03
3	sandstone	30.31	12	3627	17	17.77
3	sandstone	33.59	15	3195	16	2.25
3	sandstone	35.09	30	3108	10	73.26
3	sandstone	36.04	16	3121	19	21.16
4	granite	0.5		5851	74	0.1
4	marble	0.5		7007	189	0.1
4	limestone	6.25		5769	352	0.1
4	limestone	11.1		5019	85	0.2
4	limestone	12.2		5285	18	45
4	limestone	12.2		5437	19	45
4	limestone	12.2		5270	16	45
4	limestone	13.2		5313	15	4.5
4	limestone	13.4		4647	71	0.3
4	limestone	17.8		4593	12	380
4	limestone	17.8		4593	12	380
4	sandstone	20.3		3754	33	8
4	sandstone	20.3		3707	31	8
4	sandstone	20.3		3771	41	8
4	sandstone	20.9		3867		2040
4	sandstone	20.9		3976	48	2040
4	sandstone	20.9		3903		2040
4	sandstone	20.9		3921		2040
4	limestone	21.2		4060	57	4
4	limestone	22		3819	55	176
4	limestone	23.8		3872	11	405
4	sandstone	24.6		3572	38	58
4	limestone	26.3		3397	21	208
4	limestone	28.2		4172	18	145
4	limestone	29.2				106
4	limestone	30.8		4218	53	4
4	limestone	31.15				87
5	sandstone	21	4	4400	100	100
5	sandstone	21	4	4400	100	100
6	sandstone	17	<1	4460	65	1170.7
6	sandstone	17.1	1	4300	35	587.8
6	sandstone	22.1	1	3770	59	794.2
6	sandstone	25.9	3	3060	26	977.1